SLAC-PUB-14893
March 2012

Coherent synchrotron radiation: theory and simulations.

Alexander Novokhatski
Mail to: novo@slac.stanford.edu
SLAC National Accelerator Laboratory, 2575 Sand Hill Rd, Menlo Park, CA 94025

1.1.1 Introduction

The physics of coherent synchrotron radiation (CSR) emitted by ultra-relativistic electron bunches, known since the last century, has become increasingly important with the development of high peak current free electron lasers and shorter bunch lengths in storage rings. Coherent radiation can be described as a low frequency part of the familiar synchrotron radiation in bending magnets. As this part is independent of the electron energy, the fields of different electrons of a short bunch can be in phase and the total power of the radiation will be quadratic with the number of electrons. Naturally the frequency spectrum of the longitudinal electron distribution in a bunch is of the same importance as the overall electron bunch length. The interest in the utilization of high power radiation from the terahertz and far infrared region in the field of chemical, physical and biological processes has led synchrotron radiation facilities to pay more attention to the production of coherent radiation. Several laboratories have proposed the construction of a facility wholly dedicated to terahertz production using the coherent radiation in bending magnets initiated by the longitudinal instabilities in the ring. Existing synchrotron radiation facilities also consider such a possibility among their future plans.

There is a beautiful introduction to CSR in the "ICFA Beam Dynamics Newsletter" N 35 (Editor C. Biscari). In this paper we recall the basic properties of CSR from the theory [1-4] and what new effects, we can get from the precise simulations of the coherent radiation using numerical solutions of Maxwell's equations [5]. In particular, transverse variation of the particle energy loss in a bunch, discovered in these simulations, explains the slice emittance growth in bending magnets of the bunch compressors and transverse de-coherence in undulators. CSR may play same the role as the effect of quantum fluctuations of synchrotron radiation in damping rings. It can limit the minimum achievable emittance in the synchrotron light sources for short bunches.

1.1.2 Classical Synchrotron Radiation

It is interesting to note that exactly 100 years ago G. A. Schott [1] published a formula for an intensity of radiation of a relativistic charged particle, which makes an instantaneously circular motion. The power radiated into the n th harmonic is described by

$$\frac{dI_n}{do} = \frac{e^2 n^2}{2\pi c}\omega_0^2\left[J_n^2\left(\frac{nv}{c}\cos\theta\right)tg^2\theta + \frac{v^2}{c^2}J_n'^2\left(\frac{nv}{c}\cos\theta\right)\right] \qquad (1)$$

Submitted to ICFA Beam Dynamics Newsletter
Work supported in part by US Department of Energy contract DE-AC02-76SF00515.

where $do = \sin\theta d\theta d\varphi$, $\omega_0 = 2\pi f_0$ is a revolution frequency, v is a particle velocity, c is speed of light, e is an electron charge, J_n is a Bessel function of n-th order. Integration by solid angle gives [2]

$$I(n) = \frac{2e^2}{v}\omega_0^2\left[n\frac{v^2}{c^2}J'_{2n}\left(2n\frac{v}{c}\right) - n^2\left(1-\frac{v^2}{c^2}\right)\int_0^{v/c} J_{2n}(2n\xi)\,d\xi\right] \tag{2}$$

Finally for a continuous spectrum $dn = \frac{d\omega}{\omega_0}$ and consider only high values of n we can get an approximate formula [2]

$$I(\omega) = \frac{\sqrt{3}}{2\pi}\frac{\omega_0 e^2}{c}\left(\frac{E}{mc^2}\right)F\left(\frac{\omega}{\omega_c}\right) \qquad F(\xi) = \xi\int_\xi^\infty K_{5/3}(\eta)\,d\eta \tag{3}$$

Where $\omega_c = \frac{3}{2}\omega_0\left(\frac{E}{mc^2}\right)^3$ is a critical harmonic frequency, E is the particle energy, m is the particle mass, $K_{5/3}(\eta)$ is a modified Bessel function. Plot of the function $F(\xi)$ is shown in Fig. 1. The function reaches a maximum value at 0.29 (approximately one third of the critical frequency). Approximate formulas [2] for small and large values of ξ are:

for $\xi \ll 1$

$$F(\xi) \approx 2^{2/3}\Gamma\left(\frac{2}{3}\right)\xi^{1/3} \approx 2.15\xi^{1/3} \tag{4}$$

for $\xi \gg 1$

$$F(\xi) \approx \sqrt{\frac{\pi}{2}}\xi^{1/2}\exp(-\xi)\left[1+\frac{55}{72}\frac{1}{\xi}\right] \tag{5}$$

These approximate functions are also shown in Fig. 1.

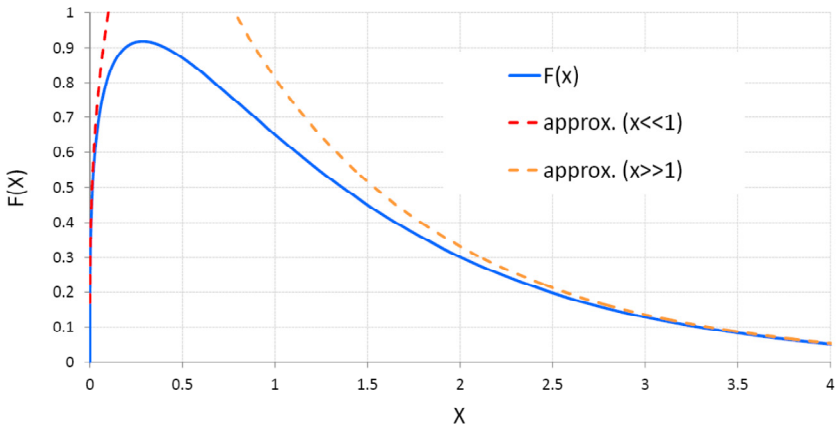

Figure 1: Function F(x) and its approximations

We can integrate the power loss spectrum over all frequencies to get the total power loss [3]

$$\frac{dE}{dt} = \int_0^\infty I(\omega)\, d\omega = \frac{2}{3}\omega_0^2 \frac{e^2}{c}\left(\frac{E}{mc^2}\right)^4 \tag{6}$$

We had the opportunity to observe experimentally this strong dependence of the energy during the SLAC B-factory operations. During the 2008 energy scan to study 2S, 3S and above 4S resonance, we need to change the energy of HER (High Energy Ring) from 8 GeV to 10 GeV. Simultaneously we measured the energy loss due to synchrotron radiation (incoherent radiation, linear with the beam current) and coherent radiation (quadratic with the beam current) of wake fields [6]. A plot of an energy loss per turn for incoherent radiation is shown at Fig. 2. A fit of the experimental data points with a power function gave an exact fourth order dependence.

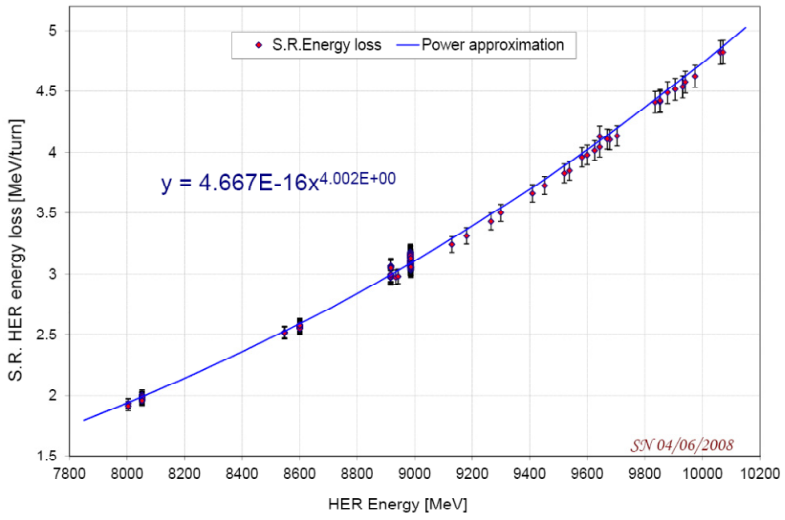

Figure 2: Measured synchrotron energy loss as a function of a beam energy.

1.1.2.1 *Coherent Radiation*

The presented formula (6) describes an energy loss of a single particle. To calculate the total loss of a bunch of particles, we need to know [3] the Fourier spectrum $j(\omega)$ of the bunch current $j(t)$

$$\frac{dE}{dt} = \int_0^\infty I(\omega)\left|j(\omega)\right|^2 d\omega \tag{7}$$

A single particle current is a δ-function in the time domain, so it has a constant value in the frequency domain $j(\omega) = 1$. If we have many particles we may assume that the total current is a sum of single particles

$$j(t) = \sum_{k=1}^{N} \delta(t - t_k) \tag{8}$$

and Fourier spectrum is

$$j(\omega) = \int j(t)\exp(i\omega t)\, dt = \sum_{k=1}^{N} \exp(i\omega t_k) \tag{9}$$

Whence

$$\left|j(\omega)\right|^2 = \sum_{k=1}^{N}\exp(i\omega t_k)\cdot\sum_{l=1}^{N}\exp(-i\omega t_l) = N + 2\sum_{k=1}^{N}\sum_{l=k+1}^{N}\cos\left(\omega(t_k - t_l)\right) \tag{10}$$

In accelerators the number of particles in a bunch is very high $N \sim 10^8 - 10^{12}$, so we can easily change a sum to an integral. If we have a function $\rho(\tau)$, which describes the particle distribution in a bunch, we can normalize this function to unity:

$$\int_{\tau_{\min}}^{\tau_{\max}} \rho(\tau)\,d\tau = 1$$

Now we change sums in the right side of (7) by integrals using this function

$$\sum_{k=1}^{N}\sum_{l=k+1}^{N}\cos\left(\omega(t_k - t_l)\right) \approx N^2 \int_{\tau_{\min}}^{\tau_{\max}} \rho(\tau_1)\,d\tau_1 \int_{\tau_1}^{\tau_{\max}} \cos\left(\omega(\tau_1 - \tau_2)\right)\rho(\tau_2)\,d\tau_2 \tag{11}$$

In this form (11) one can easily recognize a formula for the calculation of an eigenmode loss factor of a cavity, excited by a bunch passing through this cavity [7]. If we have a bunch with a Gaussian distribution and r.m.s. bunch length σ

$$\rho(t) = \frac{c}{\sqrt{2\pi}\sigma}\exp\left(-\frac{c^2t^2}{2\sigma^2}\right) \tag{12}$$

then after integrating by parts in (8) we get

$$I_b(\omega) = I(\omega)\left|j(\omega)\right|^2 = I(\omega)N\left[1 + N\exp\left(-\left(\frac{\omega\sigma}{c}\right)^2\right)\right] \tag{13}$$

The coherent part of the radiation can become noticeable in some region of a spectrum if

$$N\exp\left(-\left(\frac{\omega\sigma}{c}\right)^2\right) > 1 \quad \text{or} \quad \omega < \frac{c}{\sigma}\sqrt{\ln N} \quad \text{or} \quad f = \frac{\omega}{2\pi} < \frac{c}{2\pi\sigma}\sqrt{\ln N} \tag{14}$$

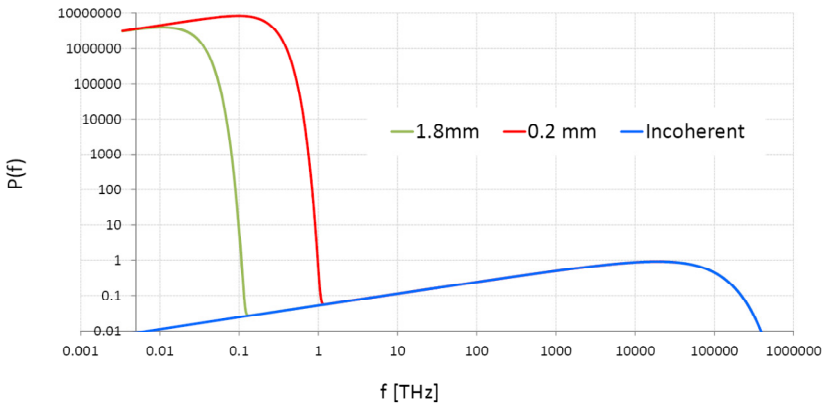

Figure 3: Power spectrum of the synchrotron radiation emitted by a 0.2 mm bunch (red line) and by a 1.8 mm bunch (green line) including incoherent radiation of a single particle (blue line).

For example the coherent part of a spectrum "touches" 1 THz when a bunch has $4\cdot10^8$ particles and its bunch length is of 0.2 mm. A critical frequency is usually much higher

than a bunch frequency, for example for a particle energy is 1.3 GeV and revolution frequency is 2.71 MHz then critical frequency $\omega_c/2\pi = 6.7\cdot 10^4$ THz. A plot of the spectrum power of the synchrotron radiation for a bunch with presented parameters is shown in Fig. 3. The coherent spectrum power level is very high; however the total power can be small. Because the main spectrum is in the region of $\omega \approx \frac{c}{\sigma} \ll \omega_c$ we can use approximation (4)

$$\begin{aligned} I(\omega) &= \frac{1}{\omega_0} I(n) \\ I(n) &\approx \frac{3^{1/6}}{\pi}\Gamma\left(\frac{2}{3}\right)\frac{\omega_0^2 e^2}{c}\cdot\left(\frac{\omega}{\omega_0}\right)^{1/3} \end{aligned} \tag{15}$$

to estimate the total coherent power

$$\frac{dE_{coh}}{dt} = N^2 \int_0^\infty I(\omega)\exp\left(-\left(\frac{\omega\sigma}{c}\right)^2\right)d\omega \approx \frac{3^{1/6}}{\pi}\Gamma^2\left(\frac{2}{3}\right)\frac{(Ne)^2}{\sigma^2}c\left(\frac{\omega_0}{c}\sigma\right)^{2/3} \tag{16}$$

To apply this formula (16) or formula (3) to an accelerator bending magnet [8] we simply hide a revolution frequency by making a change $\omega_0 = c/R$, and then the coherent power takes the form

$$\frac{dE_{coh}}{dt} \approx \frac{3^{1/6}}{\pi}\Gamma^2\left(\frac{2}{3}\right)\frac{(Ne)^2}{\sigma^2}c\left(\frac{\sigma}{R}\right)^{2/3} \tag{17}$$

This formula is very popular in the CSR study and was revised several times in modern literature [9-12]. The numerical coefficient is sometimes slightly different.

In real life bunches of electrons circulate inside a vacuum chamber of an accelerator. Usually a vacuum chamber has metal walls. This metal chamber can strongly effect the low frequency part of the radiation spectrum of a bunch. To get the analytical formulas to estimate this effect J. Swinger used the model of two parallel metal infinite plates as an approximation of a beam chamber. According to [4] the power emitted into n th harmonic is completely different:

$$I_\parallel(n) = 4\pi\frac{n\omega_0}{h}\mathrm{Re}\left\{\sum_{j=1,3,\ldots}^{\infty}\left[-H_n^{(1)}J_n + \frac{1}{2}\left(H_{n-1}^{(1)}J_{n-1} + H_{n+1}^{(1)}J_{n+1}\right)\right]\right\} \tag{17}$$

Where *h* is distance between the plates, and the argument of all the Hankel functions is

$$\xi_{n,j} = \sqrt{n^2 - \left(j\frac{\pi c}{\omega_0 h}\right)^2} = \sqrt{n^2 - \left(j/\vartheta\right)^2} \tag{18}$$

Only modes for which, $\xi_{n,j}$ is real, or $j < n\vartheta$ $\vartheta = \frac{\omega_0}{c}\frac{h}{\pi}$ can contribute to the power.

Finally a function $f_\parallel(n,\vartheta)$

$$f_\parallel(n,\vartheta) = \frac{3}{4}\frac{n}{\vartheta}\sum_{j=1,3,\ldots}^{j<n\vartheta}\left(\frac{j}{n\vartheta}\right)^4\left[K_{1/3}^2\left(\frac{j}{3\vartheta}\left(\frac{j}{n\vartheta}\right)^2\right) + K_{2/3}^2\left(\frac{j}{3\vartheta}\left(\frac{j}{n\vartheta}\right)^2\right)\right] \tag{19}$$

describes the coherent synchrotron radiation of a bunch between two metal plates [4]

$$I_{\parallel}(n) = \frac{\omega_0^2 e^2}{c} \cdot f_{\parallel}(n, \vartheta) \tag{20}$$

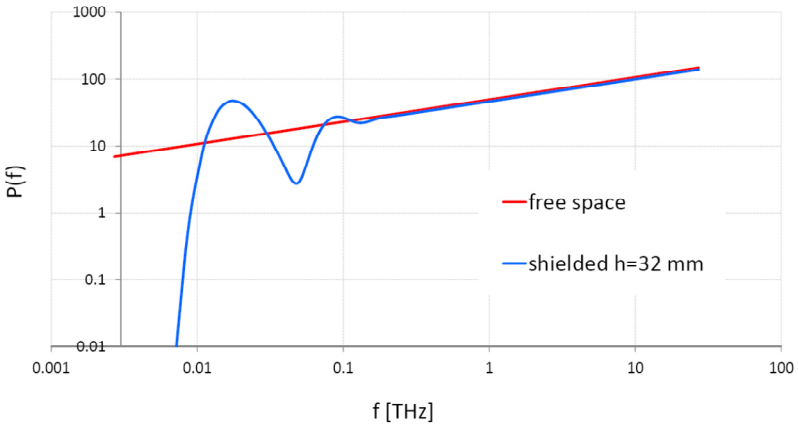

Figure 4: Comparison of the radiation power spectrum in free space and between two metal plates for the case of R=17.6 m, h=32 mm.

We have changed the numerical coefficient from 4/3 to 3/4 in formula (19) to match the radiation between two plates (20) and radiation in free space (15) at the harmonic numbers above the bunch frequency. The comparison of (20) and (15) is shown in Fig. 4. It can be seen that metal plates can not only cut the low frequency spectrum, but also increase the power at some frequencies. A fully electromagnetic simulation (which will be described in the next chapter) of the real chamber geometry shows a different result (Fig. 5).

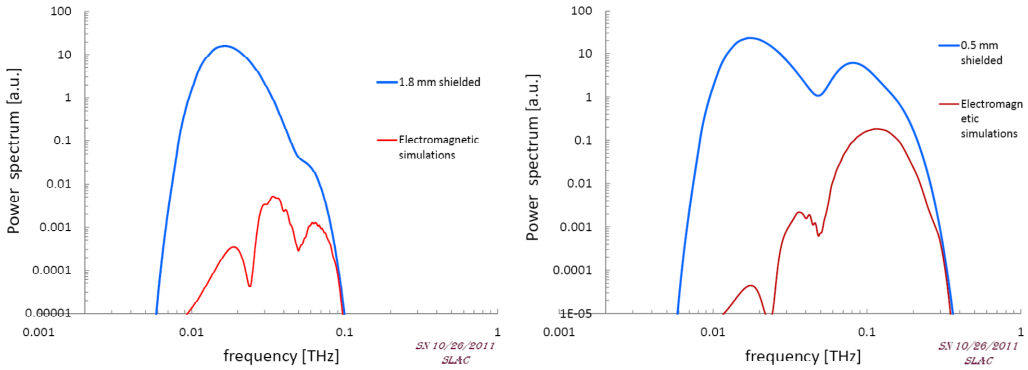

Figure 5: Comparison of the radiation of a 1.8 mm and 0.5 mm bunches between two metal plates (analytic solution, blue line) and the result of electromagnetic simulations of radiation in the taped beam chamber (red line).

Under the assumption that a bunch length l_b is comparable with the distance between plates, J. Swinger [4] got the expression for the total coherent power emitted by a bunch with a uniform charge distribution

$$\frac{dE}{dt} \approx \frac{\sqrt{3}}{2} \frac{(Ne)^2}{l_b^2} c \cdot \left(\frac{\omega_0}{c} h \right) = \frac{\sqrt{3}}{2} \frac{(Ne)^2}{l_b^2} c \cdot \left(\frac{h}{R} \right) \tag{21}$$

1.1.3 **Electromagnetic CSR simulation**

We may suggest that a direct solution of Maxwell's equations together with Newton's equations can describe the detailed structure of the CSR fields, the fields generated by an ultra-relativistic bunch of charged particles moving in a metal vacuum chamber inside a bending magnet. Electromagnetic components E, B must satisfy the equations

$$\begin{aligned} &\frac{1}{c}\frac{\partial}{\partial t}\vec{E} = \nabla\times\vec{B} - \frac{4\pi}{c}\vec{j}_b \quad \nabla\bullet\vec{E} - 4\pi\rho_b \quad \vec{E}_{wall}\times\vec{n} = 0 \\ &\frac{1}{c}\frac{\partial}{\partial t}\vec{B} = -\nabla\times\vec{E}_b \qquad \nabla\bullet\vec{B} = 0 \qquad \vec{B}_{wall}\bullet\vec{n} = 0 \end{aligned} \tag{22}$$

A charge density and a charge current must satisfy a continuity equation

$$\nabla\bullet\vec{j}_b + \frac{1}{c}\frac{d}{dt}\rho_b = 0 \quad \rho_b = \sum_k \rho_k(\vec{x}) \quad \vec{j}_b = \sum_k \rho_k(\vec{x})\vec{v}_k \tag{23}$$

A Newton force includes electromagnetic components and a bending magnetic field

$$\frac{d}{dt}\vec{p}_k = e\vec{E} + \frac{\vec{v}_k}{c}\times e\left(\vec{B} + \vec{B}_{bend}\right) \quad \vec{p}_k = m\vec{v}_k \Big/ \sqrt{1 - \frac{v_k^2}{c^2}} \tag{24}$$

Modeling ultrafast phenomena requires a special algorithm for solving the electromagnetic equations. This algorithm must be free of frequency dispersion which means that all propagating waves must have their natural phase velocity, completely independent of the simulation parameters like a mesh size or a time step. There are a lot of finite-difference schemes, which numerically solve Maxwell's equations since the first one was published in 1966 [13]. Most of them are so-called ''explicit'' schemes, which means that the value of the field at the new time step is calculated only by the field values from the previous time step. Stability conditions for these schemes do not allow a time step to be greater than or equal to a space (mesh) step. This limitation brings an additional troublesome effect for wavelengths that are comparable to a mesh step. We state that this effect works like a frequency dispersion media, which is ''hidden'' in the finite-difference equation. The main strategy of our method is to use an implicit algorithm which does not have stability issues and employs a more efficient use of finite element mesh techniques. This method can produce self-consistent stable solutions for very short bunches. The scheme could have dispersion in the transverse direction. However, electromagnetic fields, which interact with a beam, propagate in the vacuum chamber at small angles, so the effect of dispersion in the transverse direction is less important than dispersion in the longitudinal direction. We also use a Fourier expansion in the vertical direction. To decrease the amount of needed memory we use a traveling mesh. This is very important for bunch compressor simulations at higher beam energies where the bunch length is a micron but the distance between bends is tens of meters. The mesh moves with the speed of light and we can definitely assume that the electromagnetic field in front of the bunch is zero. Because the time delay due to the bending magnet in the chicane is very small, we do not need more space for the bunch. A traveling mesh does not change the accuracy of the scheme or any conditions of stability. To simulate the real shape of a non-monochromatic bunch moving, for example, in a bending magnet we will use an ensemble of particles. We will track each particle and average the current (particle velocities) over the mesh. The charge density distribution will be integrated using the continuity equation for charge and current. This will help to smooth out errors of particle transitions from one cell to another. More

details can be found in [5]. Other approaches for CSR calculations can be found in [14-16].

1.1.4 CSR field dynamics

1.1.4.1 *Radiation in a bend*

Let us first try to understand how a bunch field remakes itself when a bunch is rotated in a magnetic field. We have calculated the electromagnetic field of a three dimensional Gaussian bunch that is initially moving along the vacuum chamber very close to the speed of light. At some point the bunch enters a vertical magnetic field of a bend. What happens after can be seen at Fig. 6, where snapshots of the electric field line distributions are shown at different time moments. In these plots the white boxes with the red arrows show a bunch contour and a bunch velocity direction. Before entering a bend the bunch has only a transverse field, which can be seen as a set of vertical lines. A new field that is generated in a bend is a set of ovals, which increase in size with a time. We can outline two time periods of the field formation. The first period is when a bunch is still inside the region of its initial transverse field. The first two plots in Fig. 6 are related to this first period. The second period starts when the bunch is delayed so much that it is out of the region of the initial transverse field. The bunch is delayed because the velocity vector rotates and the longitudinal component becomes smaller and smaller than the speed of light, however field lines that are not very far away "don't know" about this change and continue to propagate at the speed of light. The last plot in Fig. 6 shows this situation. We may consider these fields to be the fields of the edge radiation in a bend.

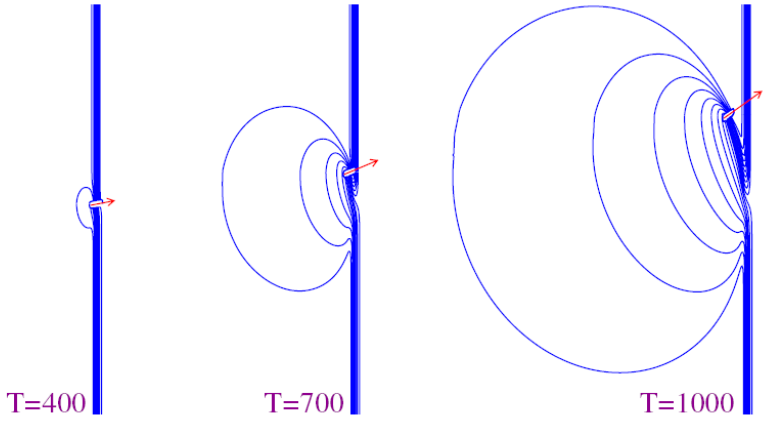

Figure 6: Snapshots of electric field lines of a bunch, which is moving in a magnetic field. White boxes show the bunch contour. Red arrows show the directions of the bunch velocity.

A more detailed picture of the field lines is shown in Fig. 7, where we also show the directions of the electric field lines by green arrows.

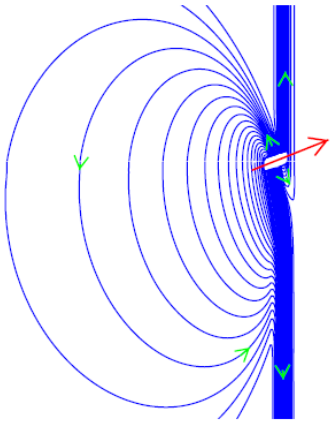

Figure 7: Detailed structure of the field pattern. Red arrow shows the direction of the bunch velocity. Green arrows show the field line direction. Upper field lines take the position of the lower lines and a part of the lower field lines take the position of the upper lines.

If one examines this picture he can see that the upper field lines take the position of the lower lines and a part of the lower field lines take the position of the upper lines. However at the far ends the transverse field lines continue traveling in the same initial direction. We can easily to explain such behavior if we present this field as a sum of two fields $\vec{E} = \vec{E}_{dp} + \vec{E}_{in}$. First field $\vec{E}_{dp}$ is the field of a dipole, which consists of two oppositely charged bunches. One bunch, which has a positive charge is the "real" one. This bunch is rotated in the magnetic field while the other bunch is a "virtual" one, which has an opposite charge and travels straight in the initial bunch direction. Second field $\vec{E}_{in}$ is the field of another "virtual", but positively charged bunch, which travels straight along the initial bunch direction. Naturally the virtual bunches together sum to zero. When we decompose the charges we decompose the fields and the very complicated structure of the radiation field becomes very simple. The decomposition of the field is shown in Fig. 8.

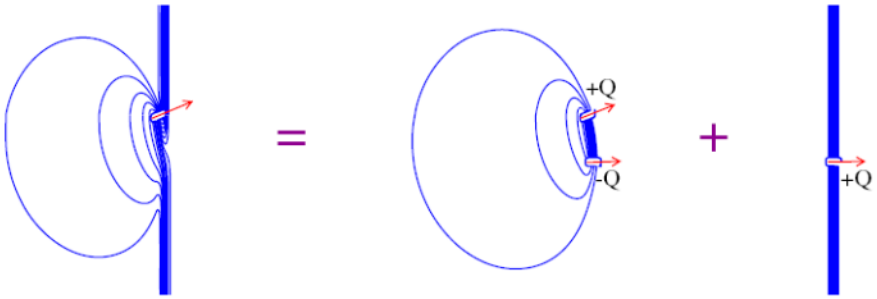

Figure 8: Decomposition of the field of a bunch moving in a magnetic field (left plot) into two fields: a field of a dipole (middle plot) and a field of a bunch moving straight in initial direction (right plot). Red arrows show directions of a bunch velocity

The interaction of the bunch with the dipole field $\vec{E}_{dp}$ continues for a longer time. Fig. 9 shows the absolute value of the electric field on the horizontal plane in the vertical center of the vacuum chamber in consecutive time steps. The white oval shows the real bunch contour. When a dipole is created an electric field appears between a real bunch and a virtual bunch. This field increases in value and reaches a maximum value when the bunches are completely separated and then it goes down as the bunches move apart leaving the fields only around the bunches. The bunch acquires an energy loss while interacting with the dipole field.

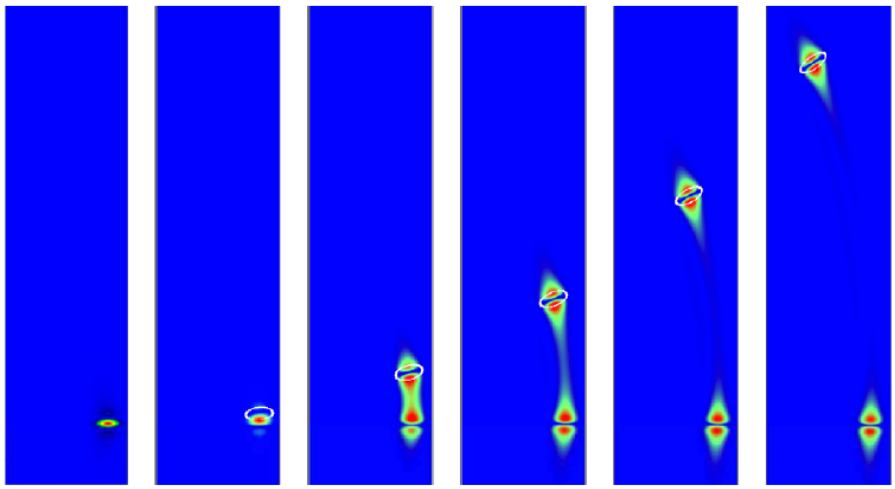

Figure 9: Absolute value of the electric field $\vec{E}_{dp}$ on the horizontal plane in the vertical center of the vacuum chamber in consecutive time steps. The red color corresponds to maximum value. The blue color corresponds to the minimum value of the field. The white oval shows the real bunch contour.

Continuing the study the radiation process we investigate a dense set of field lines in Fig. 7, a fine structure of the field in front of a bunch. This region is common with classical synchrotron radiation. We show a comparison in Fig. 10.

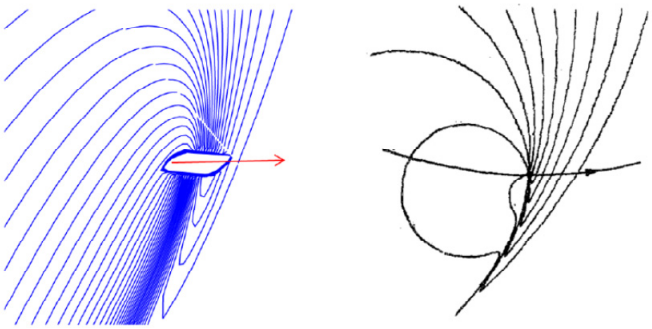

Figure 10: Fine structure of the field pattern in front of a bunch. The left plot shows field lines near a bunch. The right plot presents a picture from the reference [17].

The characteristic wavelength of the synchrotron radiation or an equivalent value of the bunch length for this relativistic factor is

$$\sigma_{s.r.} \approx \frac{R}{\gamma^3} \tag{25}$$

We chose reference [17], as it supplies a picture of the field lines of a particle with a relativistic factor γ=6. The equivalent value of the bunch length for this relativistic factor is very close to our bunch length. Fig. 10 shows this finite structure together with a plot from [17]. We can state that the region before a bunch is very close for both cases.

1.1.4.2 *Fields acting inside a bunch*

In order to study the fields acting on the particles inside the bunch we calculate the distribution of a collinear force $F_{\parallel}$ and a transverse force $F_{\perp}$ as projections to the bunch velocity

$$F_{\parallel} = \vec{J}_b \bullet \vec{E} \quad F_{\perp} = \left[\vec{J}_b \times \vec{E}\right]_x$$

We have found some very exciting fine structure of this force acting on the particle in the bunch. Fig. 11 shows a distribution of forces on the horizontal plane in the vertical center of the vacuum chamber at three time moments. The left three vertical plots in Fig. 11 show a bunch charge distribution. The starting plots are at the bottom at the time when a bunch just enters the magnetic field. The red arrows show the direction of the bunch velocity. The middle three vertical plots show a transverse force. Again, the red arrow shows the direction of the force. The transverse force is the well known space-charge force, which probably is compensated by a magnetic force in the ultra-relativistic case. The right three vertical plots show the collinear force, which is responsible for an energy gain or an energy loss. The red color corresponds to acceleration and energy gain and the blue color corresponds to deceleration or energy loss. The red arrows are collinear or anti collinear with a bunch velocity. We did not include these forces in the beam dynamics simulation in order to make the physical picture clear.

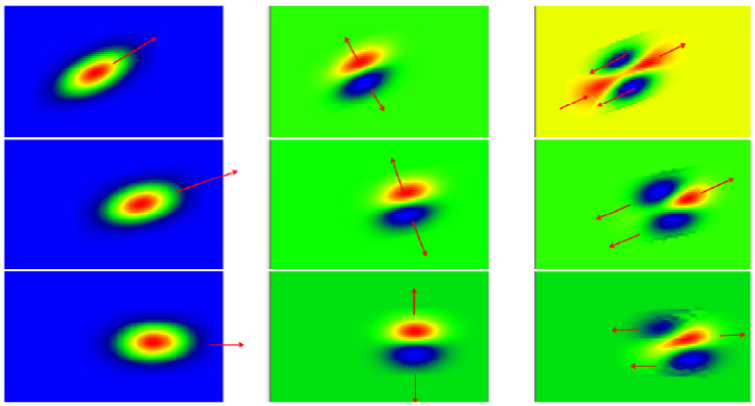

Figure 11: Bunch charge distribution, transverse forces and collinear forces on the horizontal plane in the vertical center of the vacuum chamber at three time moments. The starting plots are at the bottom at the time when a bunch just enters the magnetic field. The left three vertical plots show a bunch charge distribution. The red arrows show the direction of the bunch velocity. The middle three vertical plots show a transverse force. Again, the red arrows show the direction of the force. The right three vertical plots show the collinear force, which is responsible for an energy gain or energy loss.

We see here that the forces on the bunch are very complicated. The particles, which are in the center of the bunch, in front of the bunch and at the end are accelerated, whereas the particles at the boundaries are decelerating. This means that a bunch gets an additional energy spread in the transverse direction. The total effect is deceleration and the bunch loses energy. The asymmetry of the longitudinal fields can also be seen in Fig. 6-7, which shows the electric field line distributions. The bunch shape deformation due to the difference in the angular velocity along the radial position is usually small and can be seen only after some time; however the ultra-small beam emittance can be changed.

The integrated energy loss along the transverse direction as a function of the longitudinal coordinate is shown in Fig. 12 together with a bunch longitudinal distribution. One can see that the head of a bunch and tail are accelerated, when the rest of the bunch is decelerated. The shape of the energy loss distribution is compared with the analytical 1-D model [10] (green dashed line). We obtain a better agreement with the shape of the energy loss distribution for a larger bending radius and smaller bunch length. This comparison is shown at the right plot of Fig. 12. The transverse energy spread is smaller for a larger bending radius.

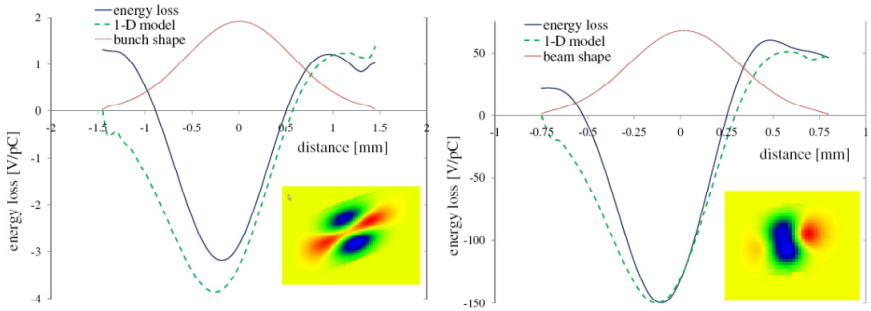

Figure12: Integrated energy loss along the transverse direction as a function of the longitudinal coordinate for two values of bending radius. The right plot shows the result for a bending radius 40 times larger and a bunch length that is two times smaller. The green dashed line is from the analytical 1-D model.

This complicated structure of the collinear field is very important. A bunch will get an additional transverse energy spread, which cannot be compensated. This energy spread in the magnetic field immediately generates emittance growth. This effect can limit the efficiency of the magnetic bunch compressors and as a result the efficiency of FELs.

1.1.4.3 *Coherent edge radiation*

As we mention above an ultra-relativistic bunch and CSR fields are moving together and interact for a long time. However one can see a field, which propagates straight

ahead from the initial beam horizontal position. This field can be seen very well when the bunch gets a large horizontal displacement. Fig. 13 shows the distribution of the magnetic field on the horizontal plane in the vertical middle of the vacuum chamber. The large peak corresponds to the bunch field. The right picture is a magnified image of the left picture. Note the scales in the X and Z directions are different A red arrow shows the initial bunch X-position and the direction of the bunch velocity. A blue arrow shows the direction of the bunch velocity at this time.

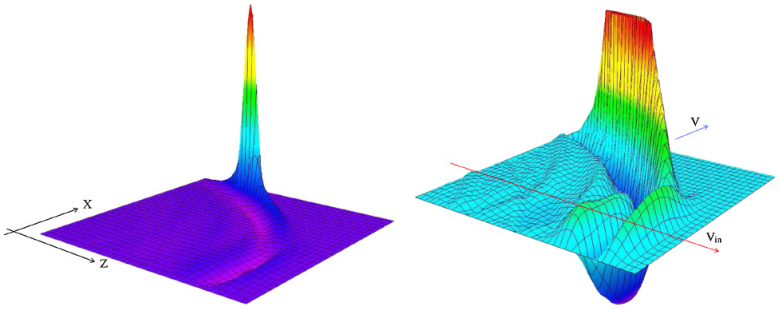

Figure13 : Coherent edge radiation. Distribution of the magnetic field on the horizontal plane in the vertical middle of the vacuum chamber. The large peak corresponds to the bunch field. The right picture is a magnified image of the left picture. Note the scales in the X and Z directions are different A red arrow shows the initial bunch X-position and the direction of the bunch velocity. A blue arrow shows the direction of the bunch velocity at this time.

Other Fig. 14 shows images of the coherent radiation in the form of transverse magnetic field distributions on the vertical planes of the vacuum chamber. The left and right sets of vertical plots correspond to different longitudinal positions. Each plot in a set shows a distribution at a different time. At first we see an image of edge radiation, then the image of synchrotron radiation and finally a bunch field image.

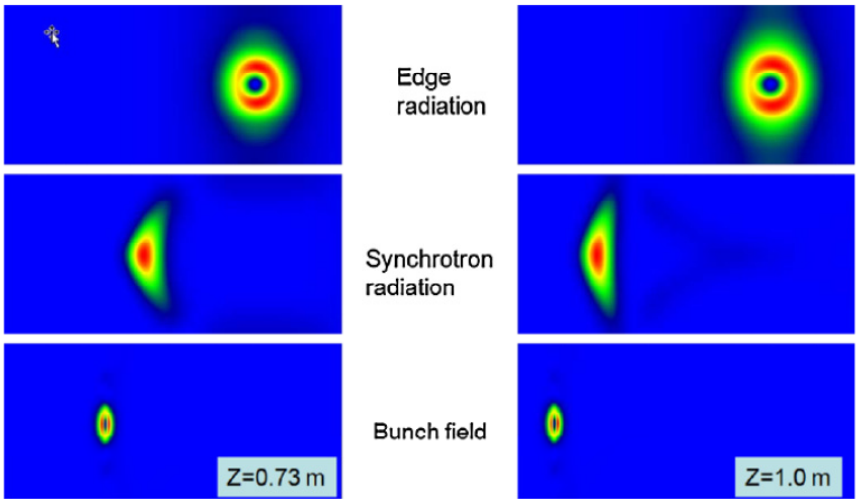

Figure 14: Images of radiation in the form of transverse magnetic field distributions. The left and right set of vertical plots corresponds to different longitudinal positions. Each plot in a set shows a distribution at a different time. The upper plot is an image of edge radiation, which appears first, the middle plot shows an image of the synchrotron radiation, which comes after and the last plot is a bunch field image.

The calculated images of the coherent edge radiation look very similar to the images, which we have seen on the YAG screen after the dump magnets, which bend the beam down at LCLS.

1.1.4.4 *Fields in the beam chamber of an accelerator*

As we mentioned before, the metal walls of a vacuum chamber of an accelerator change the distribution of the radiation fields, but the self electromagnetic field of a bunch is also modified by the chamber geometry. This field is much stronger than the radiation fields. Fig. 15 shows the vertical electric field component inside the chamber when a bunch has left a magnet. The shape of a chamber follows a bunch trajectory. To see the radiation fields we need to magnify the amplitude by 1000 times.

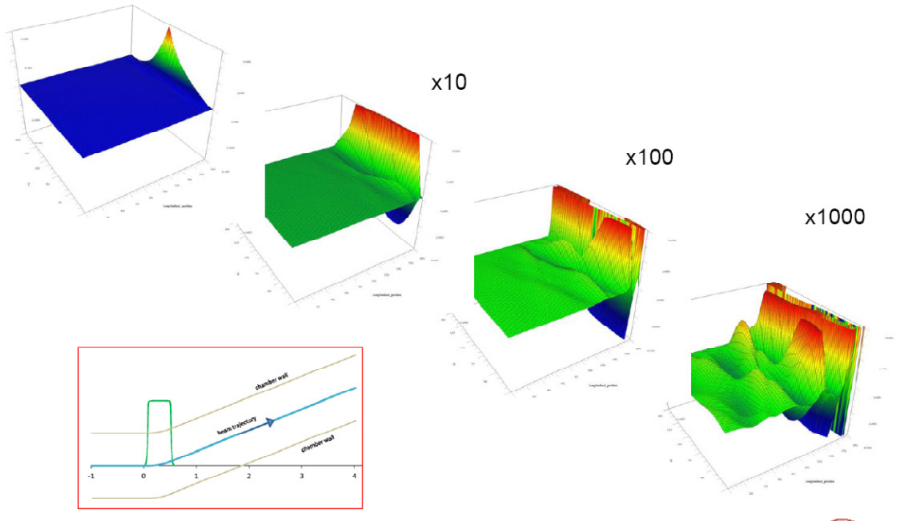

Figure 15: Magnified vertical component of the electric field of a bunch moving in the vacuum chamber after been bend by a magnet.

When a bunch changes position in a chamber, its electromagnetic field also changes and the bunch must react back: loosing and then gaining the kinetic energy. In some cases this effect can be a much stronger radiation loss. Let's return back to Fig. 5, which shows the difference in spectrum of radiation for real vacuum chamber, which is usually used in the synchrotron light sources. The horizontal size of such a chamber allows a beam to move in a circle and the edge radiation to go straight to an optical window. This tapered chamber has a lot of RF eigenmodes, which may be responsible for the complicated behaviour of the spectrums.

1.1.5 **Conclusions**

We recall well-known formulas for synchrotron radiation and analyze the fine structure of the coherent synchrotron fields, excited by a short bunch in a bending magnet. We have found that there is much more interesting and detailed structure of the CSR fields, which have not been described by any previous study. A very important result is discovering the structure of the complicated collinear force. A bunch will get

an additional energy spread in the transverse direction from the collinear force. This immediately leads to an emittance growth and decoherence that could limit FEL lasing for very short bunches. We will continue study this effect.

1.1.6 **Acknowledgments**

The author would like to thank Mike Sullivan and R. Clive Field for help and valuable comments, Franz-Josef Decker, Paul J. Emma and Yunhai Cai for support and interest in this work and physicists of the Beam Physics Department for useful discussions. This work was supported by Department of Energy Contract No. DE-AC0376SF00515

1.1.7 **References**

1. G. A. Schott, Electromagnetic Radiation, Cambridge (1912).
2. J. Schwinger, “On the Classical Radiation of Accelerated Electrons”, Phys. Rev. 75, Num 12, p. 1912 (1949).
3. L. I. Schiff, “Production of Particle Energies beyond 200 MeV”, Rev. of Sci. Instr. Vol. 7, Num. 1, p. 6 (1946)
4. J.S. Nodvick and D.S. Saxon, “Suppression of Coherent Radiation by Electrons in a Synchrotron”, Phys. Rev. 96 (1954)
5. A. Novokhatski, “"Field dynamics of coherent synchrotron radiation using a direct numerical solution of Maxwell's equations", Phys.Rev.ST Accel. Beams 14 (2011) 060707.
6. A. Novokhatski, M. Sullivan, “Loss Factor of the PEP-II Rings”, proceedings of the 11 th European Particle Accelerator Conference, Magazzini del Cotone, Genoa, Italy (2008), SLAC-PUB-13297
7. P. B. Wilson “Introduction to wake fields and wake potentials”, SLAC-PUB-4547, January 1989.
8. A. Chao, M. Tigner, “Accelerator Physics and Engineering”, World Scientific
9. P. Goldreich and D.A. Keeey, “Coherent Synchrotron Radiation”, Astrophysical Journal **170** (1971) 463
10. Ya. S. Derbenev et al., “Microbunch Radiative Tail-Head Interaction”, TESLA FEL-Report 1995-05 (1995)
11. J. B. Murphy, et al., “Longitudinal Wakefield for an Electron Moving on a Circular Orbit”, Part. Accel. 57, 9 (1997).
12. E. L. Saldin et al., “On the Coherent Radiation of an Electron bunch moving in an Arc of a Circle”, NIM, Sec. A, 417, 158 (1998).
13. K. S. Yee, IEEE Trans. Antennas Propag. 14, 302 (1966).
14. R. Li. Nucl. Instrum. Meth. Phys. Res. A, 429, 310, 1998.
15. G. Bassi et al., “Overview of CSR codes”, Nuc. Instrum. Methods Phys. Res. A, 557, pp. 189–204 (2006).
16. M. Borland, Phys. Rev. ST Accel. Beams 4, 070701 (2001).
17. S. G. Arutyunyan, Sov. Phys. Usp. 29, 1053-1057 (1986)